ISSN 0016-7029, Geochemistry International, 2006, Vol. 44, No. 11, pp. 1105–1120. © Pleiades Publishing, Inc., 2006.
Original Russian Text © G.N. Savel'eva, N.S. Bortnikov, A.A. Peyve, S.G. Skolotnev, 2006, published in Geokhimiya, 2006, No. 11, pp. 1192–1208.

Ultramafic Rocks from the Markov Deep in the Rift Valley of the Mid-Atlantic Ridge

G. N. Savel'eva [a], N. S. Bortnikov[b], A. A. Peyve [a], and S. G. Skolotnev [a]

[a] *Geological Institute (GIN), Russian Academy of Sciences, Pyzhevskii per. 7, Moscow, 119017 Russia*
e-mail: savelieva@ginras.ru

[b] *Institute of the Geology of Ore Deposits, Petrography, Mineralogy, and Geochemistry (IGEM), Russian Academy of Sciences, Staromonetnyi per. 35, Moscow, 119017 Russia*
e-mail: bns@igem.ru

Received November 19, 2004

Abstract—The paper presents materials on the composition and texture of weakly serpentinized ultrabasic rocks from the western and eastern walls of the Markov Deep (5°30.6′–5°32.4′N) in the rift valley of the Mid-Atlantic Ridge (MAR). The predominant harzburgites with protogranular and porphyroclastic textures contain two major generations of minerals: the first generation composes the bulk of the rocks and consists of $Ol_{89.8–90.4}$ + $En_{90.2-90.8}$ + $Di_{91.8}$ + *Chr* (Cr# 32.3–36.6, Mg# 67.2–70.0), while the second generation composes very thin branching veinlets and consists of $PlAn_{32–47}$ + $Ol_{74.3–77.1}$ + $Opx_{55.7–71.9}$ + $Cpx_{67.5}$ + $Amph_{53.7–74.2}$ + *Ilm*. The syndeformational olivine neoblasts in recrystallization zones are highly magnesian. The concentrations and covariations of major elements in the harzburgites indicate that these rocks are depleted mantle residues (the high Mg# of minerals and whole-rock samples and the low CaO, Al_2O_3, and TiO_2 concentrations) that are significantly enriched in trace HFSE and REE (Zr, Hf, Y, LREE, and all REE). The mineralogy and geochemistry of the harzburgites were formed by the interaction of mantle residues with hydrous, strongly fractionated melts that impregnated them. The mineralogical composition of veinlets in the harzburgites and the mineralogical–geochemical characteristics of the related plagiogranites and gabbronorites suggest that these plagiogranites were produced by melts residual after the crystallization of gabbronorites. The modern characteristics of the harzburgites were shaped by the following processes: (i) the partial melting of mantle material simultaneously with its subsolidus deformations, (ii) brittle-plastic deformations associated with cataclastic flow and recrystallization, and (iii) melt percolation along zones of the maximum stress relief and the interaction of this melt with the magnesian mantle residue.

DOI: 10.1134/S0016702906110024

INTRODUCTION

The rocks dredged from the western and eastern walls of the Markov Deep (5°30.6′–5°32.4′c N, Sierra Leone quadrangle) in the Mid-Atlantic Ridge during cruises of the Russian R/V *Akademik Nikolai Strakhov* and *Akademik Ioffe* are representative of the whole rock succession of the oceanic lithosphere: the residual mantle ultramafic rocks, diverse gabbroids, dolerites, plagiogranites (trondhjemites), granodiorites, basalts, and hydrothermally altered rocks [1, 2]. The altered gabbroids in the lower part of the eastern wall contain sulfide mineralization: stringer-disseminated and massive copper sulfides [2, 3]. The Fe–Ti gabbro in the area have an U–Pb zircon age of 97.4 ± 0.15 Ma [4].

The fresh harzburgites (which are in places practically devoid of serpentine and contain no more than 10% of this mineral) were the first fresh varieties found on the Atlantic seafloor during the long-term study of its oceanic rocks (which are usually strongly serpentinized ultramafics that locally contain as much as 80–100% serpentine [5–10]). Very weakly serpentinized residual peridotites were also recently found by a German–American expedition in the Gakkel Ridge [11].

The extremely weak alterations of the ultramafics, a feature rare even in ophiolitic complexes, provides the possibility of studying their textures, mineralogy, and geochemistry without any additional limitations imposed by serpentinization and submarine weathering. Our research was based on this analysis conducted with the aim to reproduce the evolutionary history of the weakly serpentinized peridotites during slow spreading and to answer the question as to why these rocks remained practically unaltered and whether there are any significant differences between their composition and texture and those of diverse serpentinized peridotites from the same ridge segment.

Microprobe analyses of minerals (on Camebax microprobes at the Geological Institute, Russian Academy of Sciences, and Vernadsky Institute of Geochemistry and Analytical Chemistry, Russian Academy of Sciences) were conducted after the petrotextural studying of these rocks. Their microscopical examination allowed us to identify a number of generations of their

rock-forming minerals. Chemical analyses of the rocks for major and some trace (Ni and Cr) elements were carried out by X-ray fluorescence at a laboratory of the Institute of the Geology of Ore Deposits, Petrography, Mineralogy, and Geochemistry, Russian Academy of Sciences. Trace elements and REE were determined by ICP-MS on a PQ-2 (V.G. Elemental) mass spectrometer at a laboratory of the Institute of the Geology of Ore Deposits, Petrography, Mineralogy, and Geochemistry, Russian Academy of Sciences.

GEOLOGICAL SETTING OF THE ULTRAMAFIC ROCKS

The MAR segment between the Bogdanov and Strakhov fracture zones (5°–7°10′N) lies immediately south of the ridge segment intersected by thick and closely spaced fracture zones (Arkhangelskii, Vernadskii, and Doldrums). The relatively narrow rift zone extends in this segment as a single structure, which is bounded in the west and east by flattened plateaus with thick sedimentary deposits. The dissected topography of the ridge near the rift valley is typical of slow-spreading centers [12, 13]. Nontransform offset zones divide the ridge into three en-echelon segments, in which all mantle and crustal rock complexes of the oceanic crust are exposed [1, 14]. The area is characterized by low seismic activity [15], and the local gravitational maxima roughly coincide with exposures of ultramafic rocks and gabbro [16]. The area, which is a transition zone between the structures of the North and South Atlantic, is characterized by the absence of linear magnetic anomalies.

Ultramafic rocks and gabbro compose the walls and, partly, the floor of the rift valley, whereas basalts (which are dominated by evolved, highly magnesian rocks of the *N*-MORB type) are widespread in the flanks of the ridge and, locally, along the rift valley floor.

Ultramafic rocks were lifted from depths of 3600–3240 m (Site I1060) in the western wall and from depths of 3900–3600 m (Site I1063) in the eastern wall of the rift valley (Fig. 1). The material obtained at each of the sites was dominated (~70–80%) by various gabbro and dolerites and contained subordinate amounts (~20%) of ultramafics: lherzolites, harzburgites, and rare samples of dunites and websterites, including their plagioclase-bearing varieties. Most of the ultramafic rocks are 80–90% serpentinized and only occasional harzburgite fragments (no larger than a few decimeters across) bear <10% serpentine. The extensively deformed and metamorphosed rocks (~10%) are ultramafic mylonites, gneissose gabbro, chlorite–serpentine–talc and serpentine–amphibole schists, serpentinites, sheared and amphibolized gabbroids that grade into amphibolites, and diaphthorized, brecciated, and cataclased gabbro. Plagiogranites were found in the form of angular fragments up to 15 cm in both walls of the rift valley. Sulfide ore mineralization is associated with hydrothermally altered rocks.

Our concepts concerning the stratigraphy of the oceanic crust in the Markov Deep area are illustrated in Fig. 2. The insets show the reproduced vertical sections of the rock complexes and demonstrate the presence of plagiogranite (gabbro–plagiogranite) veins and veinlets in practically all of the rocks and the variations in their morphology and mineralogy in various host rocks up the stratigraphic section (Fig. 2). The harzburgites contain very thin (from a few parts of a millimeter to a few millimeters) branching veinlets, whereas the banded gabbro often bears zonal veins up to a few centimeters thick. The amphibole-bearing veins with variable morphologies of their contacts with the host gabbronorites contain partly resorbed xenoliths of the host rocks. A large plagiogranite fragment caries a xenolith of melanocratic amphibolite. The systematic variations in the morphology of the veins seem to reflect the different depths at which these veins were produced and the intensification of the segregation of the melts up the vertical lithospheric section. The occurrence of the same minerals (quartz, sphene, apatite, zircon, Fe–Ti amphibole, ilmenite, and sulfides) in all of the veins and veinlets can be interpreted as evidence of their origin from the same parental melt at different depths, when small portions of the percolating melt interacted with the residual ultramafic rocks prior to the crystallization of this melt in veins hosted in Fe–Ti gabbro and dolerites.

PETROGRAPHY

The weakly altered ultramafic rocks occur as angular and angular–rounded fragments no larger than 10 × 15 cm, with very thin (1–2 mm) yellowish weathering crusts. The harzburgites consist of 80–85% olivine, 15–20% enstatite, and single grains of diopside and Cr-spinel about 1.5%. Two lherzolite samples contain up to 5–7% diopside. Reticulate α-chrysotile veinlets (without magnetite) developed unevenly and account for 3–10% rock by area in thin sections. The rocks have coarse- to large-grained protogranular textures that grade into porphyroclastic textures. Large (5–7 mm) olivine grains are weakly elongated and possess numerous kink bands (due to intercrystalline deformations), which were produced by the translational gliding of dislocations (Fig. 3a). The enstatite usually forms single tabular grains ranging from 3–4 to 6 mm. The rocks only occasionally contain linear aggregates of pyroxene grains, which mark the directions of the subsolidus solid-plastic flow in residual harzburgites and lherzolites. The absence of pyroxene aggregates and the abundance of olivine grains with a high thickness of dislocations, including variably oriented kink bands, can be indicative of the partial recrystallization of the rocks during high-temperature deformations in a variable strain field. The cores of enstatite grains bear diopside lamellae, which are often deformed. The marginal portions of large enstatite grains are partly recrystallized with the development of equant neoblasts. Anhedral Cr-

spinel grains (0.5–1.5 mm) are associated with enstatite, with both minerals sometimes forming linear aggregates.

The protogranular texture of the rocks is perturbed by (i) the recrystallization of olivine into aggregates of grains 1–2 mm across, with randomly oriented relict kink bands and (ii) by branching or linear recrystallization and mylonitization zones, which range from a few fractions of a millimeter to 4 mm in thickness and cut across large olivine and enstatite grains with traces of intracrystalline deformations (Fig. 3b). In these zones, olivine and enstatite neoblasts range from 0.003–0.005 to 0.01–0.1 and even 0.3 (occasionally up to 0.3–0.5 mm) in size. Parallel to the boundaries of the zones, cryptogranular crushed olivine material alternates with thin- and small-grained neoblasts (Fig. 3b).

The thickest (2–4 mm) zones include veinlets of the following composition: tabular plagioclase in the central part and brown amphibole in association with sulfides and ilmenite in the margins. Plagioclase is sometimes associated with apatite, sphene, and fine-grained pleochroic clino- and orthopyroxene (Fig. 3c). Yellowish green pyroxenes are also contained in the inner contact zones of large veinlets, among recrystallized primary olivine and enstatite. The brown amphibole is locally replaced by pale green actinolite.

MINERAL CHEMISTRIES

The early-generation olivine, which occurs in the form of large grains (protogranular), is highly magnesian ($Mg^{\#}$ = 89.8–90.4) and contains 0.24–0.55% NiO and usually <0.1% CaO. Linear and branching zones cutting large grains contain recrystallized olivine in the form of equant neoblasts of a younger (relative to the protogranular olivine) generation. The mineral has a composition analogous to that of large olivine grains or is slightly more magnesian. In mylonitization zones that cut domains with recrystallized olivine at contacts with plagioclase (+ amphibole) veinlets, small olivine grains of the youngest generation are relatively low magnesian ($Mg^{\#}$ = 74.3–77.1) and contain up to 0.45% CaO (Table 1).

Large grains of magnesian ($Mg^{\#}$ = 90.2–90.8%) enstatite of an early generation are characterized by a low Al_2O_3/Cr_2O_3 ratio (equal to 3) because of their relatively high Cr_2O_3 contents (0.8–2.1%), as is typical of large enstatite grains in serpentinized peridotites from the same MAR segment (Peyve et al, 2003) (Table 2,

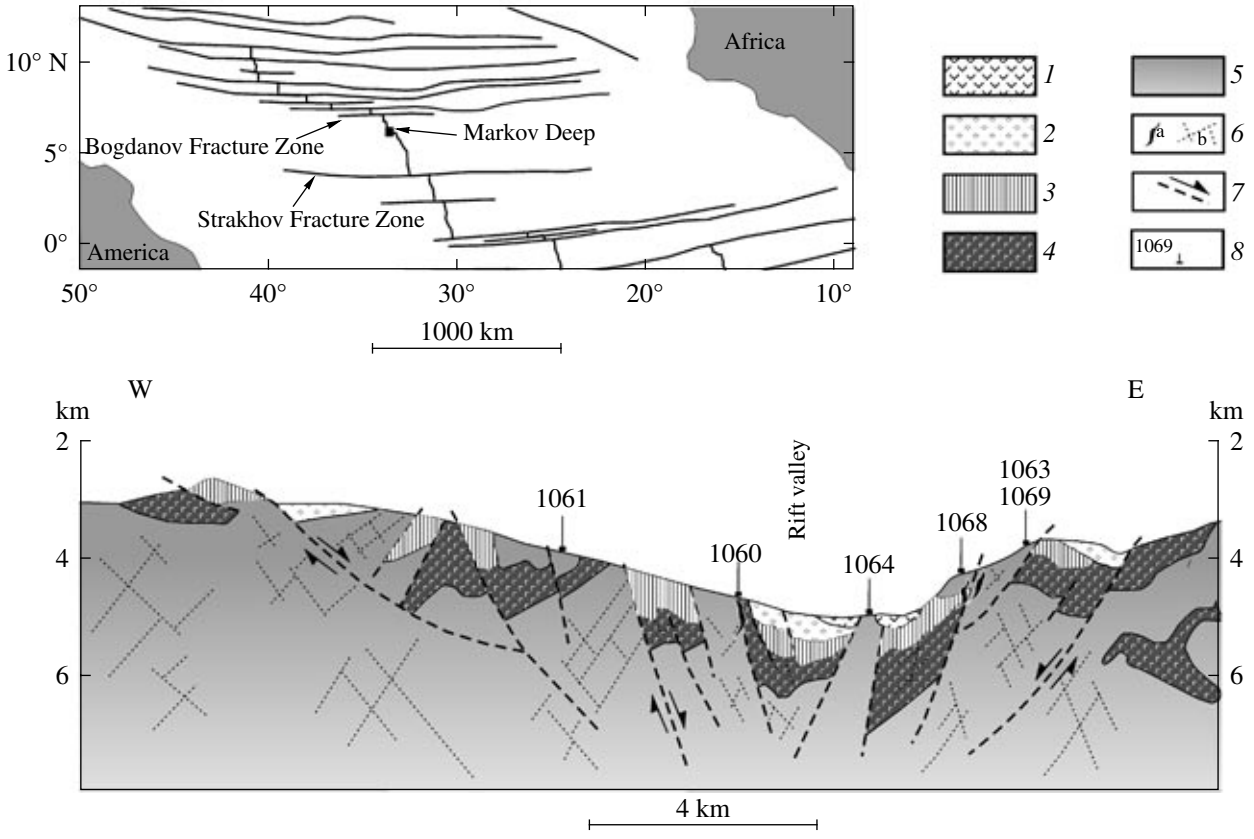

Fig. 1. Location map of the Markov Deep and geological profile across the MAR rift valley in the area [1]. (*1*) Fresh basalts; (*2*) basalts metamorphosed to the prehnite–pumpellyite and chlorite–epidote subfacies of the greenschist facies; (*3*) dolerites; (*4*) gabbroids; (*5*) residual ultramafic rocks; (*6*) (a) plagiogranites and (b) fracture zones; (*7*) listric normal faults and the displacement directions along them; (*8*) dredging sites of the R/V *Akademik Nikolai Strakhov* [2].

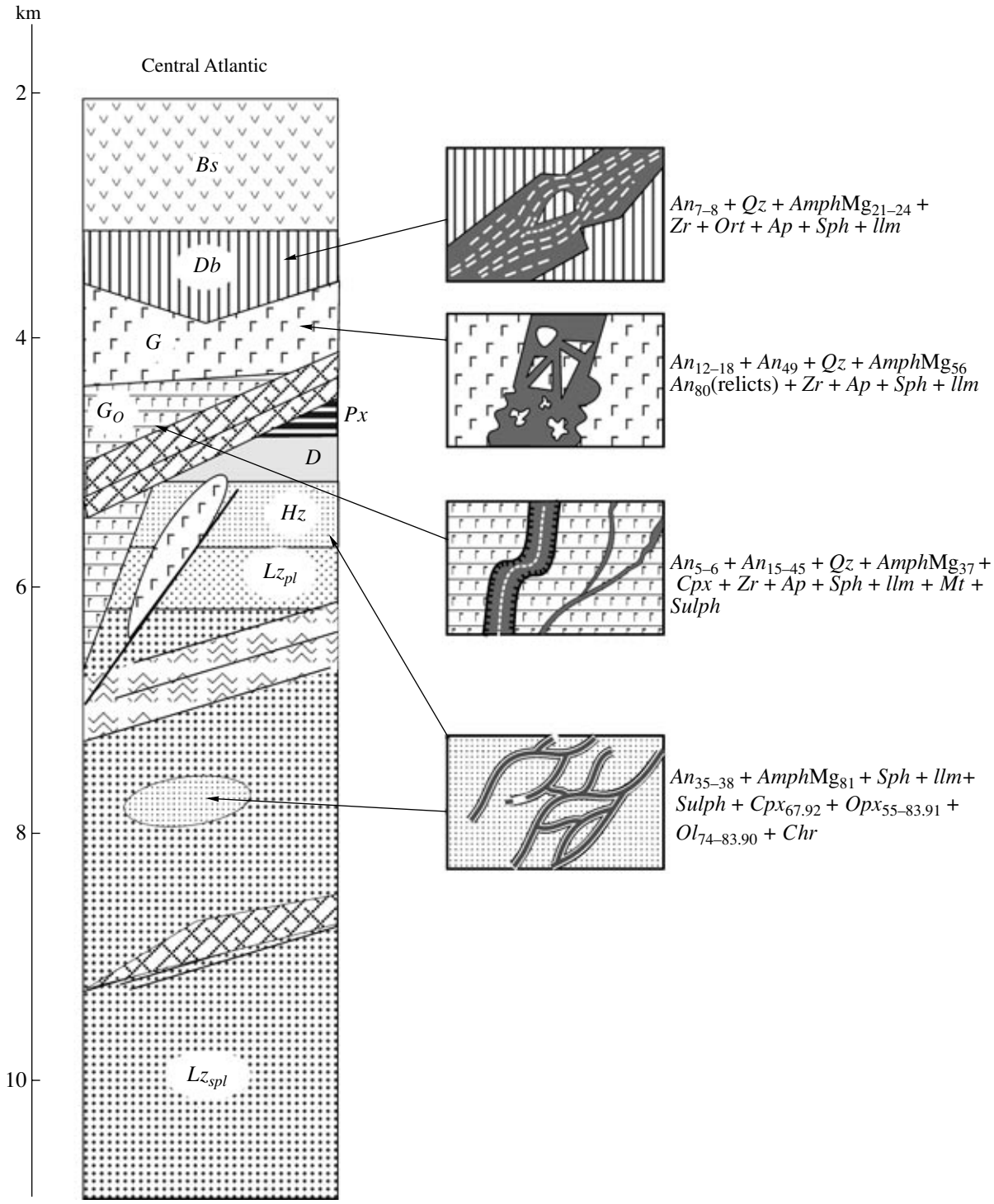

Fig. 2. Schematic vertical section of the oceanic crust in the Markov Deep area, MAR, and the setting of plagiogranites and gabbrodiorites in this section. The insets show the successive changes in the morphology of plagiogranite veins and their mineralogy up the stratigraphic section. Abbreviations: *Bs*—basalts, *D*b—dolerites, *G*—amphibole-bearing gabbro and gabbronorites, *Go*—layered olivine gabbro and troctolites, *Px*—pyroxenes, *Hz*—harzburgites, *Lz pl*—plagioclase lherzolites, *Lz spl*—spinel lherzolites. Mineral symbols (here and below, numerals correspond to Mg#): *Opx*—orthopyroxene, C_{Px}—clinopyroxene, *Amph*Mg—amphibole, *An*—plagioclase, numerals correspond to the anorthite content, *Qz*—quartz, *Zr*—zircon, *Ap*—apatite, *Sph*—sphene, *Chr*—Cr-spinel, *Ilm*—ilmenite, *Sulph*—sulfides.

Figs. 4 and 5). Small enstatite grains in the veinlets and at contacts with them are ferrous ($Mg^{\#}$ = 55.7–71.9) and very poor in Al_2O_3 (0.36%) and Cr_2O_3 (0.05%). The occurrence of orthopyroxene of this composition only in cutting veinlets and only in association with ferrous olivine, ferrous clinopyroxene, plagioclase, and amphibole led us to ascribe this variety to a younger generation of the minerals $Ol + Pl + Opx \pm Cpx \pm Amph$.

The clinopyroxene occurs as single small grains of diopside in association with Cr-spinel. Judging from the high $Mg^{\#}$ (91.8) and high Al_2O_3 (4.29%) and Cr_2O_3 (1.56%) contents, as well as from the occurrence of the mineral in rocks with an undisturbed protogranular texture, this pyroxene belongs to the early mineral association of the residual harzburgites (Table 3). The clinopyroxene in veinlets and at their contacts is principally different from diopside in the harzburgites in having a lower $Mg^{\#}$ = 67.5, lower concentrations of Al_2O_3 (1.25%), and very low contents of Cr_2O_3 (0.3%) (Table 3). This clinopyroxene, which is accompanied by small grains of ferrous olivine, orthopyroxene, and other minerals of the veinlets, was attributed to a younger generation of the minerals.

The Cr-spinel is anhedral and subhedral and has intermediate Cr# (32.3–36.6%) and $Mg^{\#}$ (62.7–70.0), low TiO_2 concentrations, and very low Fe_2O_3 concentrations (<1%) (Table 4, Fig. 6). The low degree of Fe oxidation makes the Cr-spinel of these harzburgites remarkably different from this mineral in the serpentinized ultramafic rocks.

The very thin veinlets extending along recrystallized zones are dominated by small (0.2–0.4 mm) plagioclase ($An_{32–47}$) grains of equant tabular habit. The amphibole, which is prone to be spatially restricted to the marginal portions of the veinlets, is high-temperature hornblende with high TiO_2 concentrations (3.3–3.6%), variable and generally low $Mg^{\#}$ (53.7–74.2), and high Al_2O_3 concentrations (9.46–15.27%) (Table 3). Ferrous olivine and pyroxenes from the veinlets and at their contacts (which were described above in comparison with the minerals of the harzburgites) were included in the same young generation with the plagioclase, brown Fe–Ti hornblende, and ilmenite. Ilmenite occurs as large anhedral and subhedral grains among plagioclase crystals. The high TiO_2 concentrations (51–53%) and relatively high MgO concentrations (1.2–2.0%) in this ilmenite suggest that it crystallized from a strongly differentiated residual basic melt that percolated through the harzburgites. The high TiO_2 concentration in the melt gave rise to the crystallization of large euhedral crystals of sphene in the central parts of the veinlets (Fig. 2c, Table 4). The sulfides are small euhedral crystals of pyrite and subhedral grains of pyrrhotite and, perhaps, pentlandite, which are associated with brown amphibole.

Thus, the weakly serpentinized harzburgites contain two major mineral assemblages: (i) $Ol_{89.8\text{-}90.4}$(I) + $En_{90.2–90.8}$ + $Di_{91.8}$ + *Chr*, which composes the bulk of the rocks, and (ii)$PlAn_{32–47}$ + $Ol_{74.3–77.1}$(II) + $Opx_{55.7–71.9}$ +

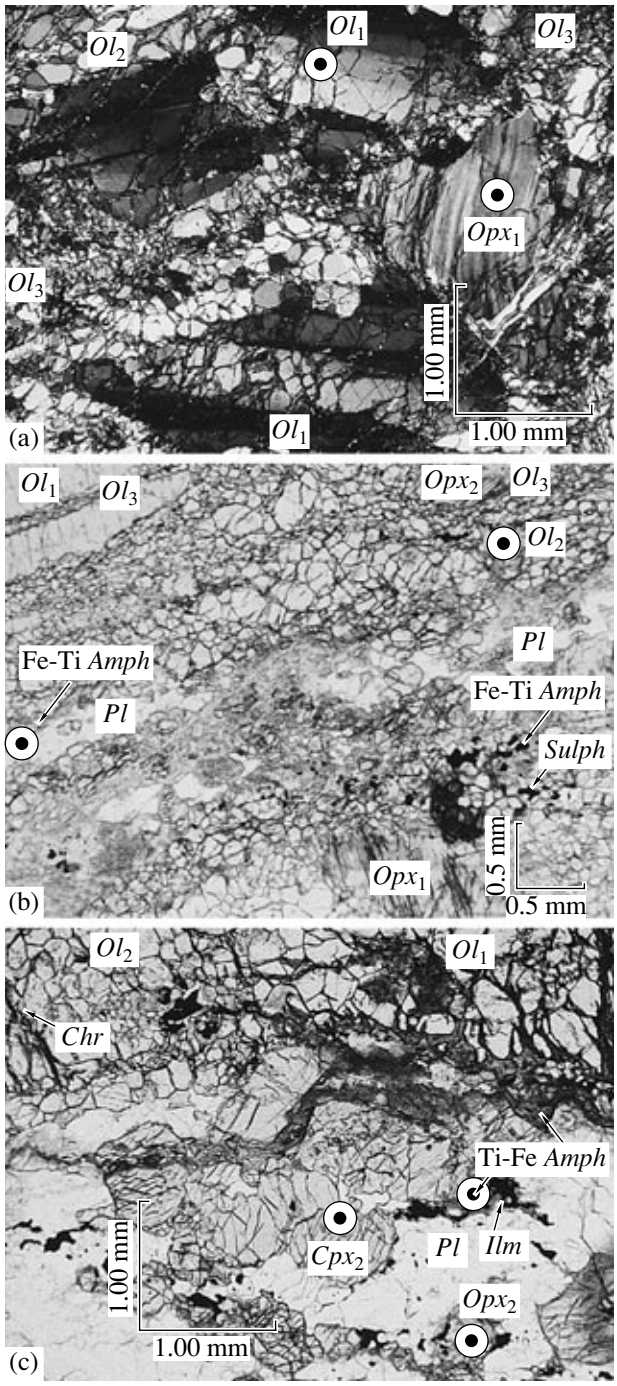

Fig. 3. Micrographs of fresh harzburgites: (a) protoolivine grains with kink bands and early recrystallization. Crossed polarizers, thin section of sample 1053-28. (b) Younger recrystallization and cataclastic flow zones. Parallel polarizers, thin section of sample 1063-30. (c) Veinlet of plagioclase and amphibole along recrystallization zones. The contacts of the veinlet are marked by newly formed grains of pyroxene and ilmenite with a rim of Ti-hornblende. Parallel polarizers, thin section of sample 1063-32. Circles correspond to microprobe spot analyses reported in Tables 1–4.

Table 1. Representative analyses of olivine in ultramafic rocks and gabbro (1069-24) from the Markov Deep, Central Atlantic

Oxide	1063-28	1063-34	1063-35	1068-44-4	1063-30	1063-32	1069-24
SiO_2	41.24	40.85	40.88	41.02	38.07	38.29	39.98
TiO_2	0.02	0.07	0.00	0.06	0.00	0.00	0.00
Cr_2O_3	0.00	0.00	0.09	0.09	0.00	0.00	0.00
Al_2O_3	0.18	0.00	0.00	0.01	0.05	0.00	0.08
FeO	9.75	9.51	9.55	9.25	23.25	21.02	13.52
MnO	0.14	0.21	0.11	0.13	0.16	0.36	0.14
MgO	48.19	48.39	48.58	48.80	37.65	39.70	45.77
CaO	0.08	0.11	0.45	0.08	0.17	0.04	0.16
Na_2O	0.00	0.00	0.09	0.01	0.22	0.04	0.00
NiO	0.35	0.55	0.24	0.53	0.22	0.54	0.34
Total	99.95	99.68	99.99	99.97	99.79	99.99	99.99
Mg#	89.81	90.07	90.07	90.39	74.27	77.10	85.78

Note: Samples 1063-28, 1063-34, and 1063-35 are fresh harzburgites without discernible veinlets; samples 1063-30 and 1063-32 are fresh harzburgites with thin amphibole–plagioclase veinlets; samples 1068-44 and 1068-45 are serpentinized lherzolites.

Table 2. Representative analyses of orthopyroxene in ultramafic rocks from the Markov Deep, Central Atlantic

Oxide	1063-28		1063-34		1063-35	1068-44-4	
	core	margin	1	2	1	1	2
SiO_2	55.47	56.11	55.28	56.02	55.82	55.66	55.43
TiO_2	0.00	0.01	0.06	0.02	0.00	0.06	0.00
Cr_2O_3	1.04	0.79	1.18	0.70	0.80	0.74	0.59
Al_2O_3	3.60	3.68	3.57	2.62	3.42	3.20	3.47
FeO	5.74	6.18	6.20	6.10	5.89	6.49	6.35
MnO	0.10	0.21	0.20	0.20	0.11	0.00	0.09
MgO	30.26	32.26	32.11	33.10	32.77	32.31	32.69
NiO	0.02	0.00	0.22	0.31	0.37	0.23	0.21
CaO	3.73	0.76	0.98	0.82	0.73	1.04	1.17
Na_2O	0.00	0.00	0.00	0.00	0.00	0.00	0.01
K_2O	0.02	0.00	0.03	0.02	0.10	0.08	0.00
Total	99.99	100.00	99.82	99.90	99.99	99.79	100.00
Mg#	90.38	90.29	90.23	90.63	90.84	89.88	90.17
Oxide	1063-32	1069-7					
	1	1	2	3	4	5	6
SiO_2	51.24	54.65	56.45	55.29	55.29	55.96	56.17
TiO_2	0.24	0.07	0.04	0.00	0.16	0.13	0.04
Cr_2O_3	0.05	1.11	0.66	0.99	1.07	0.41	0.84
Al_2O_3	0.36	3.49	2.85	3.45	3.51	2.77	2.76
FeO	26.79	5.30	5.77	6.39	5.99	6.08	6.11
MnO	0.72	0.19	0.12	0.00	0.02	0.23	0.08
MgO	18.90	30.04	32.98	32.15	32.20	33.59	32.59
NiO	0.15	0.16	0.23	0.24	0.21	0.14	0.07
CaO	1.50	4.74	0.91	1.25	1.53	0.64	1.35
Na_2O	0.04	0.25	0.00	0.25	0.00	0.00	0.00
K_2O	0.02	0.00	0.00	0.02	0.04	0.04	0.00
Total	100.00	100.00	100.00	100.00	100.00	100.00	100.00
Mg#	55.70	90.99	91.05	89.97	90.55	90.78	90.49

Table 3. Representative analyses of clinopyroxene and amphibole in ultramafic rocks and gabbro (1069-24) from the Markov Deep, Central Atlantic

Oxide	Clinopyroxene											Amphibole	
	1063-34		1068-44	1069-24	1069-7						1063-32	1063-30-3	
	1	2	1	1	1	2	3	4	5	6	1	1	2
SiO_2	51.72	52.89	51.69	53.10	51.71	52.14	52.18	52.47	51.97	51.53	52.12	43.83	45.69
TiO_2	0.00	0.14	0.14	0.31	0.07	0.05	0.07	0.11	0.06	0.07	0.40	3.30	3.57
Cr_2O_3	1.56	0.91	1.15	0.78	1.44	1.03	0.83	0.98	1.07	1.12	0.03	0.32	0.23
Al_2O_3	4.29	2.85	4.20	2.36	4.50	3.64	3.70	3.64	3.85	4.21	1.25	10.46	10.5
FeO	2.48	2.24	2.79	5.16	2.52	2.07	2.30	2.89	2.35	2.59	11.52	15.27	9.46
MnO	0.00	0.17	0.09	0.08	0.05	0.16	0.21	0.13	0.05	0.14	0.41	0.17	0.1
MgO	15.67	16.83	16.04	18.46	15.98	16.62	16.44	17.52	16.58	16.40	13.44	12.12	15.5
NiO	0.29	0.18	0.08	0.09	0.09	0.20	0.00	0.05	0.19	0.28	0.10	nd	nd
CaO	23.88	23.68	23.71	19.19	23.60	23.79	24.15	22.14	23.83	23.29	20.67	11.21	11.61
Na_2O	0.00	0.10	0.03	0.29	0.00	0.26	0.12	0.00	0.00	0.32	0.06	2.94	3.03
K_2O	0.06	0.02	0.11	0.06	0.04	0.04	0.01	0.08	0.05	0.05	0.01	0.20	0.26
Total	100.00	100.00	100.00	99.88	100.00	100.00	100.00	100.00	100.00	100.00	100.00	99.81	99.96
Mg#	91.84	93.04	91.11	86.43	91.88	93.47	92.70	91.53	92.63	91.85	67.53	57.93	75.78

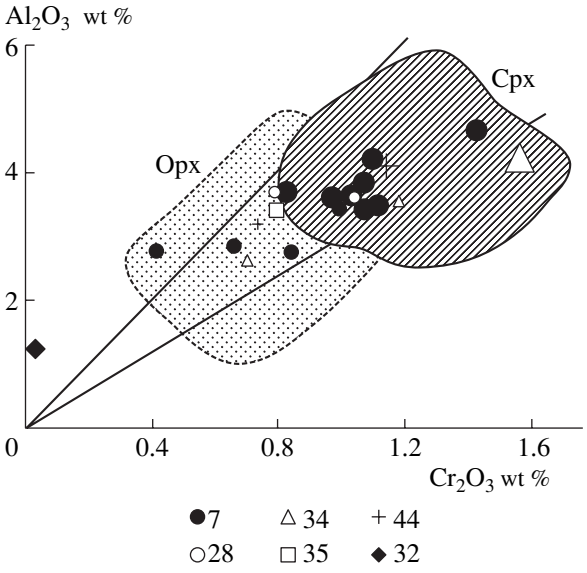

Fig. 4. Proportions of Al_2O_3 and Cr_2O_3 (wt %) in ortho- and clinopyroxene from peridotites whose whole-rock compositions are listed in Table 7. The dashed and solid lines contour the compositional fields of ortho- and clinopyroxene, respectively, from serpentinized peridotites of the Sierra Leone quadrangle (Peyve et al. 2003). Dredging sites: (2) I1069-7, (28)–I1063-28, (34)–I1063-34, (35)–I1063-35, (44)–I1068-44, (32)–I1063-32. Small and large symbols correspond to ortho- and clinopyroxene, respectively.

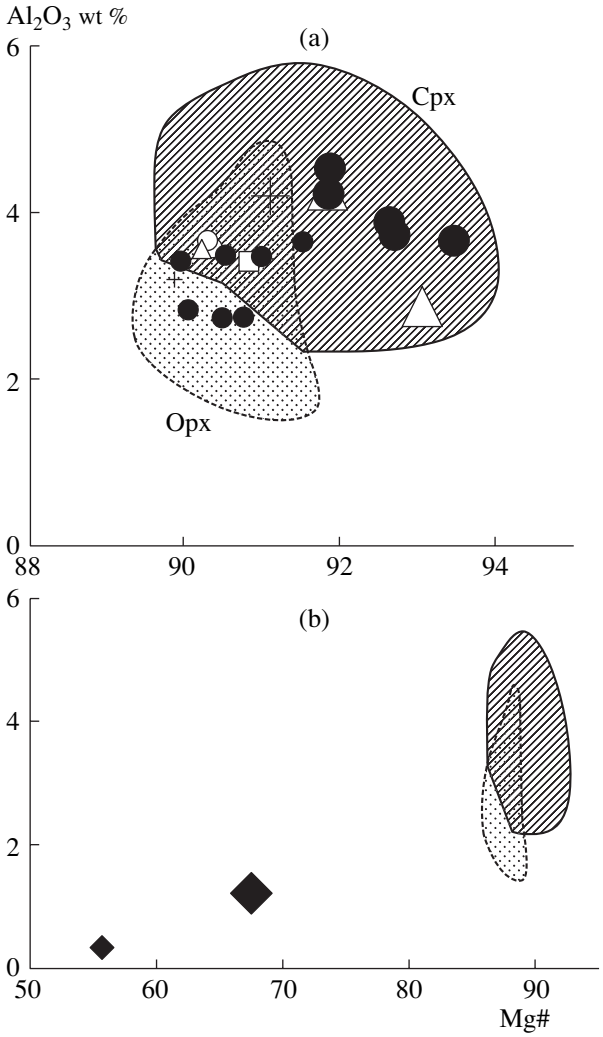

Fig. 5. Correlation between the Al_2O_3 concentration (wt %) and $Mg^{\#}$ of ortho- and clinopyroxene from (a) peridotites and (b) gabbro (solid diamonds) and peridotites (shaded fields). See Fig. 4 for symbol explanations.

$Cpx_{67.5}$ + $Amph_{53.7–74.2}$ + *Ilm*, which occurs in very thin branching veinlets. Syndeformational olivine neoblasts that developed along recrystallization zones before the origin of the veinlets are highly magnesian and have a composition analogous to that of the protoolivine.

ROCK CHEMISTRIES

The chemical compositions of the rocks are reported in correlation with the textural and mineralogical characteristics of these ultramafics. Table 5 presents analyses of the weakly serpentinized ultramafic rocks without visible amphibole–plagioclase veinlets, analogous rocks with rare thin veinlets (detected in thin sections), and serpentinized lherzolites. In all of the rocks, their relatively high $Mg^{\#}$ 89.1–89.9; (89.1 and 87.7 for the serpentinized lherzolites, samples 1068/45 and 1068/44, respectively) and the low concentrations of CaO, Al_2O_3, and TiO_2 are fully consistent with the aforementioned mineralogical features of these rocks. In the diagrams in Fig. 7, which characterize the mantle depletion trend, the data points of the rocks plot within the field of abyssal peridotites [17, 18] and depleted harzburgites with low Al_2O_3/SiO_2 = 0.01–0.02 and Al_2O_3/CaO of approximately 1.0. The serpentinized lherzolites 1068/44 and 1068/45 are the least depleted ultramafic rocks among all of the analyzed varieties, but they contain notably less CaO and Al_2O_3 than abyssal peridotites: 0.5–1.65 and 0.39–1.27% against 3–3.5 and 3.5–4.5% CaO and Al_2O_3, respectively. According to the experimental data [19] and the results of geochemical simulations [20], rocks of this composition can be produced during the partial melting of lherzolite in the presence of an aqueous fluid, after the fractionation of 15–18% of the melt. The low concentrations of TiO_2 (0.01–0.02%) and the high contents of Ni (1281–1993 ppm) and Cr_2O_3 (0.18–0.36%) in the harzburgites are comparable with the concentrations of these elements in abyssal and ophiolitic depleted residues [7, 18, 21]. Judging from the concentrations of chemically bound water in the rocks and with regard for the amounts of amphibole and talc in recrystallization zones and thin veinlets, the amount of serpentine varied from 3 to 20%, which is in general agreement with petrographic observations.

The geochemical characteristics of these rocks are more complicated. Their conspicuous feature is high concentrations of trace elements and REE in all of the fresh and serpentinized peridotites: the sum of REE

Table 4. Representative analyses of ore minerals in ultramafic rocks from the Markov Deep, Central Atlantic

Oxide	Cr-spinel						
	1063-28		1063-34		1063-35		1068-44
	1	2	1	2	1	2	1
SiO_2	0.08	0.00	0.04	0.05	0.10	0.07	0.01
TiO_2	0.14	0.04	0.13	0.11	0.00	0.04	0.05
Cr_2O_3	32.23	31.44	29.17	30.03	28.67	28.75	27.92
Al_2O_3	37.45	37.84	39.75	38.28	40.34	39.67	39.89
FeOsum	13.48	13.28	14.38	14.39	13.55	14.26	15.01
Fe_2O_3	0.66	1.53	0.67	1.49	0.98	1.61	2.47
FeO	12.88	11.90	13.78	13.05	12.67	12.81	12.79
MnO	0.08	0.21	0.27	0.34	0.16	0.15	0.09
MgO	16.43	16.71	15.82	16.06	16.62	16.43	16.40
NiO	0.11	0.41	0.20	0.11	0.21	0.28	0.43
Total	100.07	99.93	99.76	99.37	99.65	99.65	99.80
Mg#	69.45	69.45	67.17	68.68	70.05	69.57	69.57
Cr#	36.60	36.60	32.98	34.48	32.28	32.71	31.95

Oxide	Cr-spinel					Ilmenite	
	1069-7					1063-30-3	1068-32
	1	2	3	4	5	1	1
SiO_2	0.00	0.01	0.07	0.15	0.10	0.13	0.04
TiO_2	0.03	0.02	0.05	0.12	0.02	53.07	51.00
Cr_2O_3	30.38	29.13	28.54	29.39	29.39	0.07	0.29
Al_2O_3	38.77	39.59	39.82	39.71	39.21	0.03	0.00
FeOsum	14.58	14.24	14.94	14.28	14.43	42.66	45.80
Fe_2O_3	0.90	1.35	1.60	0.57	1.22	–	–
FeO	13.77	13.03	13.50	13.77	13.33	–	–
MnO	0.14	0.07	0.11	0.00	0.22	1.42	0.70
MgO	15.83	16.39	16.23	16.24	16.07	1.99	1.22
NiO	0.07	0.31	0.00	0.01	0.24	0.25	0.24
Total	99.80	99.76	99.76	99.90	99.68	99.62	99.29
Mg#	67.19	69.15	68.18	67.76	68.23	–	–
Cr#	34.45	33.05	32.46	33.18	33.45	–	–

ranges from 1.55 ppm (sample 1063/28) to 4.35 ppm (sample 1063/30) (Tables 6 and 7, Figs. 8 and 9). As the sum of REE decreases, the La/Yb and La/Sm ratios notably increase, i.e., the relative La concentration increases (for example, in sample 1063/28). The relatively high concentrations of LREE cause clearly pronounced U-shaped morphologies of the REE pattern, as is typical of mantle residues in some areas in the Atlantic and also in some ophiolite massifs [22–24]. Very low (sometimes below the detection limit) Eu concentrations were detected in four (of the five) samples of the fresh harzburgites and are also relatively low in the serpentinized lherzolites. Our data are principally different from the REE patterns of residual ultramafic rocks from the Lanzo Massif in the Western Alps, which display a clearly pronounced systematic increase in concentrations from LREE to HREE [25]. Peridotites with analogous characteristics are ascribed to so-called impregnated mantle residues [25].

The Sm/Nd and Lu/Hf ratios of the analyzed ultramafic rocks are close to or lower than those in the depleted mantle (Fig. 9b), and the Sm/Yb ratio of

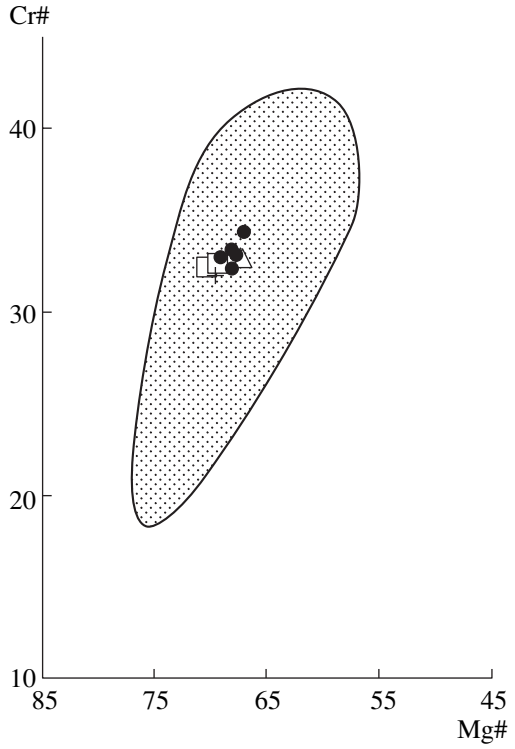

Fig. 6. Correlation between the $Cr^{\#}$ and $Mg^{\#}$ of accessory Cr-spinel from peridotites. The line contours the compositional field of accessory Cr-spinel from serpentinized peridotites from the Sierra Leone quadrangle [1]. See Fig. 4 for symbol explanations.

almost all of the rocks (except sample 1063/30) is analogous to this ratio of the depleted mantle [26]. The relatively high (Sm/Nd)cn ratio [27], which varies from 1 to 3.9, approaches the values interpreted as resulting from high degrees of melting of mantle peridotites in plume MAR segments [23].

The concentrations of Rb, Sr, Y, Zr, Nb, Hf, Ta, and Pb significantly vary, and the Zr concentrations are notably elevated (Table 6). These variations are associated with clearly pronounced positive correlations in the Zr–Hf and Zr–Yb pairs and with weaker positive correlations between Zr and Nb (Figs. 10a–10c). The direct correlations between these low-mobile elements and the high REE and Zr concentrations in the ultramafic rocks can be interpreted as a result of the interaction of the high-Mg residue with a percolating melt, a process that determined the final composition of the harzburgites. This idea finds further support in the fact that the composition of the plagiogranites dredged in association with weakly serpentinized harzburgites and composing veinlets and veins in all rocks of the succession is also characterized by very high REE concentrations (up to 180 ppm La and 210 ppm Zr in sample 1060/57). The clearly pronounced Eu minima in the chondrite-normalized REE patterns (Fig. 11) of the plagiogranites suggest that they crystallized from a melt

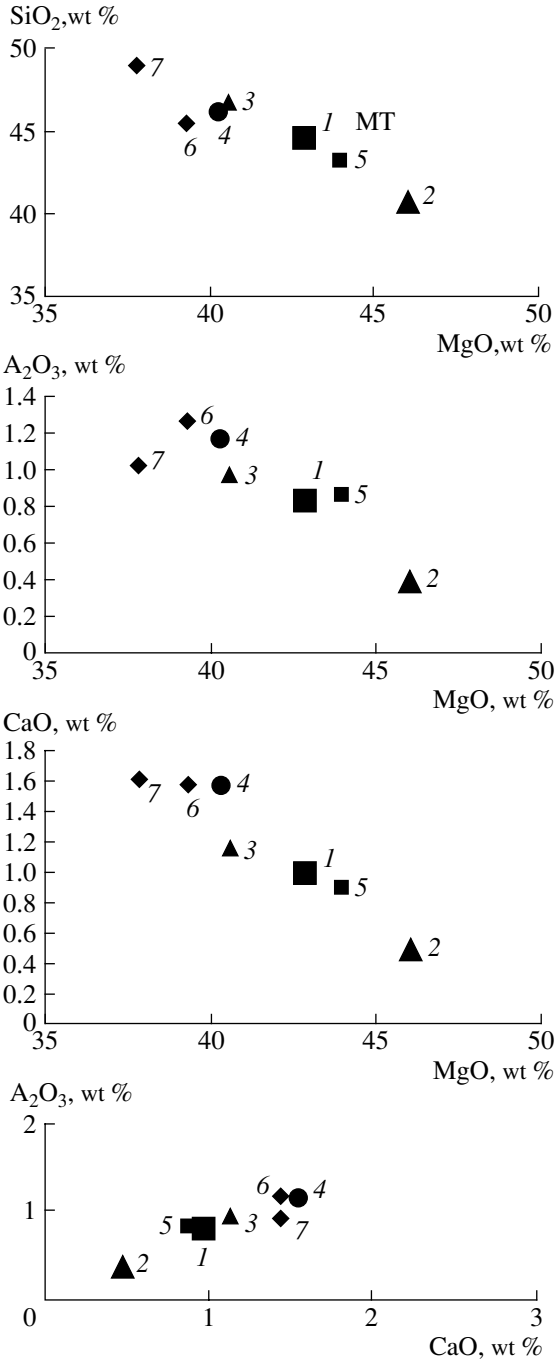

Fig. 7. Variations in the bulk compositions of ultramafic rocks demonstrate an increase in the MgO concentrations with decreasing SiO_2, Al_2O_3, and CaO, in compliance with the mantle depletion trend, and the concurrent decrease in the Al_2O_3 and CaO concentrations from lherzolites to harzburgites. Numerals near symbols correspond to the numbers of analyses in Table 5.

complementary to gabbroids with high-Ca plagioclase, which are also present in the rock succession.

There is no correlation between the concentrations of mobile large-ion elements (Sr and Hf, Ba and Rb), and the concentrations of these elements display the

Table 5. Bulk-rock composition of ultramafic rocks and gabbro from the Markov Deep, Central Atlantic

Oxide, %	Ultramafic rocks							Gabbro
	1	2	3	4	5	6	7	8
	1063-28	1063-30	1063-32	1063-34	1063-35	1068-44	1068-45	1069-24
SiO_2	44.77	40.89	47.03	46.46	43.45	45.73	49.20	46.70
TiO_2	0.02	0.01	0.02	0.02	0.02	0.06	0.02	0.06
Cr_2O_3	0.83	0.39	0.98	1.18	0.86	1.27	1.02	20.90
Al_2O_3	9.58	11.27	9.17	9.38	9.82	10.98	9.24	5.28
FeO	8.63	10.14	8.25	8.44	8.83	9.88	8.31	4.75
MnO	0.14	0.15	0.13	0.14	0.15	0.17	0.15	0.07
MgO	43.03	46.25	40.76	40.47	44.16	37.99	39.77	14.00
CaO	1.01	0.50	1.18	1.59	0.91	1.59	1.62	11.69
Na_2O	0.06	0.08	0.06	0.07	0.07	0.07	0.06	1.13
P_2O_5	0.01	0.01	0.00	0.00	0.00	0.00	0.00	0.00
K_2O	0.04	0.02	0.03	0.04	0.03	0.02	0.00	0.02
Ni	0.26	0.30	0.23	0.25	0.26	0.23	0.25	0.05
Cr	0.19	0.09	0.35	0.37	0.22	0.34	0.34	0.05
S	0.04	0.04	0.04	0.03	0.03	0.07	0.12	0.03
LOI	3.73	3.90	3.80	1.40	3.77	9.67	10.01	3.76
Total	99.61	99.49	98.69	98.32	99.03	100.38	98.25	99.94
Mg#	89.90	89.10	89.80	89.50	89.90	87.70	89.10	89.00

Note: The analyses were conducted by XRF at a laboratory of the Institute of the Geology of Ore Deposits, Petrography, Mineralogy, and Geochemistry (IGEM), Russian Academy of Sciences. See Table 1 for rock names.

most significant variations. The behavior of these components was likely controlled by the active participation of a fluid phase in the processes of medium- and low-temperature metamorphism [28]. It is worth mentioning the higher concentrations of Sr and Rb (which are elevated by factors of 5–10) in the fresh harzburgites compared to those in the serpentinized lherzolites and the higher concentrations of Ba and Cs, which are below the detection limits in the serpentinized rocks. The contents of such metals as Cu, W, and Ta are, conversely, notably higher in the serpentinized lherzolites (Table 6).

DISCUSSION

Summarizing the materials presented above, we will discuss the geological setting of the rocks, their texture and composition (which can shed light onto the nature of and the reasons for the occurrence of weakly altered residual ultramafic rocks on the seafloor and make it possible to reproduce some aspects of their evolutionary history and genesis).

The geological setting of the weakly altered ultramafic rocks is noted for the fact that the spreading of the oceanic crust over the past 1.5–2 Ma in the Sierra Leone quadrangle was associated only with the eruptions of thin basaltic flows [1]. Intense multistage deformations affected various deep lithospheric levels, including the root zones of nontransform offsets, when deep-sitting rocks were brought to the surface and the oceanic crustal rock succession was formed. Traces of deformations are clearly discernible in the residual ultramafic rocks and plutonic gabbroids. The same rocks and dolerites are impregnated by younger, strongly differentiated residual melts in the form of veins and thin veinlets of plagiogranite and leucogabbro–diorite composition. Thus, the local crust was not produced during a single stage, and the plagiogranite that are younger than the rock succession of residual ultramafic rock—layered gabbro—dolerite interlink and chronologically "seal" the oceanic crustal and, perhaps, also uppermost lithospheric succession.

The microtextures of the ultramafic rocks provide evidence of more than one stage of their deformations. The earliest stage left traces in the form of intercrystal-

Table 6. Concentrations (ppm) of trace elements in ultramafic rocks from the Markov Deep, Central Atlantic

Element	1063-28	1063-30	1063-32	1063-34	1063-35	1068-44	1068-45	1069-24
Co	98.11	115.00	102.00	76.47	95.80	86.18	92.20	38.70
Ni	1738.00	1993.00	1579.00	1281.00	1673.70	1384.70	1637.50	497.80
Cu	0.54	5.72	3.26	6.91	0.57	16.66	31.86	54.56
Zn	38.10	62.90	42.20	46.00	50.90	44.66	54.16	245.30
Ga	0.95	0.78	1.52	0.69	1.22	1.34	1.18	8.86
Rb	4.50	4.29	0.46	3.12	5.32	0.71	0.59	6.56
Sr	14.52	24.51	1.59	12.05	26.41	2.02	3.71	165.40
Y	0.46	1.42	0.52	0.61	0.94	0.97	0.71	1.17
Zr	4.10	7.62	12.32	4.21	17.25	13.53	21.06	11.37
Nb	0.17	0.26	0.14	0.15	0.27	0.74	0.37	0.23
Mo	0.00	2.06	0.49	2.54	0.20	0.24	0.27	0.00
Ag	6.54	7.76	7.98	4.33	10.54	4.38	5.10	8.30
Sn	12.59	0.00	0.00	0.00	28.58	0.00	0.00	40.97
Sb	0.27	0.14	0.15	0.31	0.14	0.29	0.49	0.43
Cs	0.63	1.18	0.00	0.54	22.00	0.00	0.00	0.06
Ba	656.00	1172.00	11.95	724.70	1430.60	0.00	0.00	2027.30
Hf	0.17	0.37	0.55	0.15	0.69	0.63	0.92	0.48
Ta	0.97	0.95	0.96	0.14	0.37	19.64	5.84	1.96
W	2.53	6.95	567.60	16.19	2.05	160.80	268.20	0.00
Au	0.08	0.04	0.06	0.18	0.23	0.89	0.63	0.21
Pb	1.76	0.56	0.61	3.03	1.20	2.17	3.41	4.22
Th	0.12	0.15	0.06	0.40	0.11	0.10	0.19	0.13
U	0.20	0.13	0.13	0.11	0.19	0.14	0.40	0.08
Zr/Y	8.91	5.37	23.69	6.90	18.35	13.95	29.66	9.72
Zr/Y	8.91	5.37	23.69	6.90	18.35	13.95	29.66	9.72
Zr/Nb	24.12	29.31	88.00	28.07	63.89	18.28	56.92	49.43
Ta/Hf	5.71	2.57	1.75	0.93	0.54	31.17	6.35	4.08

Note: The analyses were conducted by ICP-MS at a laboratory of the Institute of the Geology of Ore Deposits, Petrography, Mineralogy, and Geochemistry (IGEM), Russian Academy of Sciences (analysts S.A. Gorbacheva, V.D. Sidel'nikova, and L.S. Tsimlyanskaya).

line gliding in olivine crystals with subparallel kink bands oriented nearly perpendicular to the direction in which dislocations moved in the crystals. The high-temperature brittl-plastic deformations of the ultramafics were initially induced under dry subsolidus conditions and proceeded during normal faulting, as follows from the anhydrous syndeformational mineral assemblages: the first generation of neoblasts (0.5–0.8 mm) of high-Mg olivine and, more rarely, orthopyroxene that developed along kink bands. The first generation of relatively large syndeformational neoblasts was formed at temperatures of 1180–1050°C (according to the Cr/Al thermometer [19]), at a low stress (within 40–60 MPa), which was evaluated from the sizes of the neoblasts and their crystallization temperature [29, 30], and, correspondingly, at low deformation rates. The next stage was responsible for the development of linear zones of recrystallization and plastic flow, which contain olivine neoblasts from 0.005–0.08 to 0.1–0.2 mm. With regard for the sizes of these neoblasts, their magnesian composition, and the cutting position with respect to the predominant direction of the glinting bands in the protoolivines, it is reasonable to conclude that the differential stress and deformations rate drastically increased, and the strain field changed [29–32]. The syndeformational olivine–enstatite (diopside) mineral assemblage in the youngest transecting (mylonite) zones was produced at T = 980–850°C, under a stress, which was also assayed from the sizes of the neoblasts and their crystallization temperatures at 100–270 MPa.

After this, the migration of a fluid/melt initiated in these zones resulted in the origin of plagioclase, Ti-rich amphibole, ferrous clinopyroxene, ilmenite, sulfides,

Table 7. Concentrations (ppm) of REE in ultramafic rocks from the Markov Deep, Central Atlantic

Element	1063-28	1063-30	1063-32	1063-34	1063-35	1068-44	1068-45	1068-24
La	0.30	0.40	0.20	0.20	0.40	0.30	0.40	0.40
Ce	0.50	0.80	0.40	0.50	0.60	0.70	0.70	0.50
Pr	0.09	0.25	0.04	0.09	0.16	0.10	0.09	0.11
Nd	0.04	1.10	0.20	0.40	0.70	0.40	0.40	0.50
Sm	0.05	0.25	0.3	0.08	0.14	0.11	0.4	0.17
Eu	nd	nd	nd	nd	0.07	0.03	0.01	0.19
Gd	0.07	0.28	0.06	0.07	0.15	0.15	0.06	0.22
Tb	0.02	0.04	0.01	0.01	0.02	0.02	0.01	0.02
Dy	0.11	0.30	0.07	0.12	0.21	0.20	0.10	0.24
Ho	0.02	0.06	0.02	0.02	0.04	0.04	0.02	0.04
Er	0.07	0.21	0.08	0.07	0.15	0.15	0.12	0.13
Tm	0.02	0.03	0.02	0.02	0.03	0.03	0.02	0.02
Yb	0.07	0.21	0.10	0.10	0.20	0.18	0.13	0.14
Lu	0.02	0.05	0.03	0.02	0.05	0.04	0.03	0.04
Hf	0.17	0.37	0.55	0.15	0.69	0.63	0.92	0.48
Total	1.55	4.35	1.81	1.85	3.61	3.08	3.05	3.20
Lu/Hf	0.12	0.14	0.05	0.13	0.07	0.06	0.03	0.08
Sm/Nd	1.25	0.23	0.15	0.20	0.20	0.28	0.10	0.34
La/Yb	4.29	1.90	2.00	2.00	2.00	1.67	3.08	2.86

Note: The analyses were conducted by ICP-MS on a PQ-2 (V.G. Elemental) mass spectrometer at a laboratory of the Institute of the Geology of Ore Deposits, Petrography, Mineralogy, and Geochemistry (IGEM), Russian Academy of Sciences.

and sphene. Near the veinlets, the magnesian protoolivine and enstatite were replaced by more ferrous generations: $Mg^{\#}$ changed from 90.8 to 86.3 for olivine and from 91.9 to 71.9 for enstatite.

The general analysis of the data presented above suggests that the composition of the ultramafic rocks was determined by the following processes: (i) the partial melting of mantle material associated with subsolidus deformations; (ii) high-temperature brittle–plastic deformations accompanied by cataclastic flow and local recrystallization along linear zones; and (iii) melt percolation along zones where the stress relief was at a maximum.

The composition of the weakly altered ultramafics is unusual in that these rocks are depleted mantle residues in terms of major elements (highly magnesian minerals and bulk-rock compositions and low concentrations of Ca, Al, and Ti) and, at the sate time, are strongly enriched in trace HFSE and REE, particularly in Zr, Hf, Y, LREE, as well as the in sum of REE. There can be several reasons for these inconsistencies between the major- and trace-element and REE compositions of these rocks.

The plausible explanations of these reasons should take into account the fact that the rocks are closely associated with plagiogranites, and some of the harzburgites contain very thin amphibole–plagioclase veinlets. The plagiogranites are noted for high concentrations of Zr, Y, and LREE. During the percolation of melts through these harzburgites, the rocks should have become enriched in these elements. In an open system with melting, percolating melt interacts with the residue, extracts and removes some components from it, and introduces others [33–36]. This process is associated with the enrichment of the residues in low-mobile HFSE and LREE. Moreover, the very high concentrations of certain trace elements, such as Th, Ta, U, and, in some samples, also Rb and, particularly, Ba, the elevated concentrations of all REE, as well as the presence of high-temperature amphibole and the diversity of the accessory and ore minerals in the veinlets, testify that the melts that impregnated the peridotites were hydrous and strongly fractionated. The geochemical characteristics of the plagiogranites described above (for example, their Eu minimum) suggest that these rocks crystallized from residual melts complementary with the gabbronorites that contain Fe–Ti amphibole.

If the partially melted material consisted of garnet lherzolites or a mixture of spinel lherzolites and garnet pyroxenites (melting in a mantle column approximately 50 km thick [20]), it is also reasonable to expect an

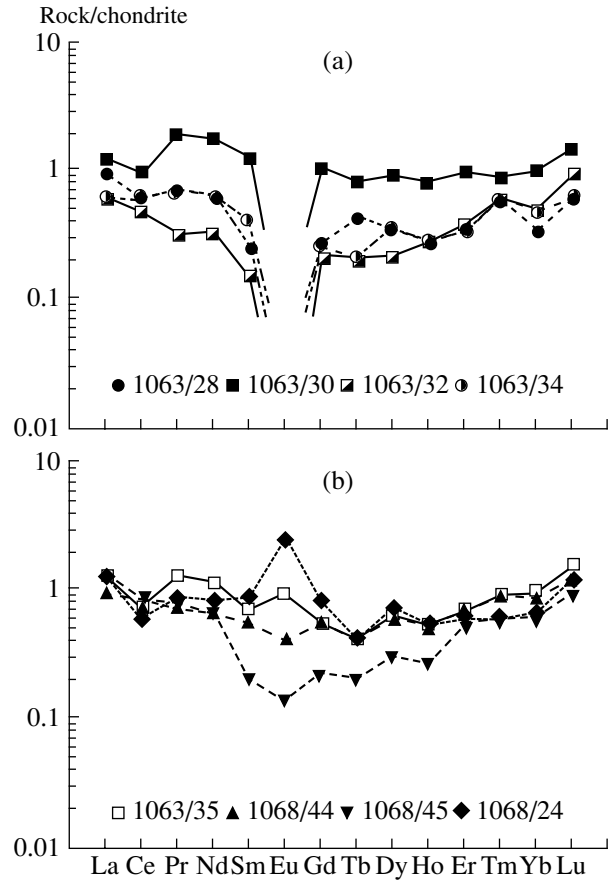

Fig. 8. Chondrite-normalized (Sun and McDonough, 1989) REE patterns of peridotites. Samples: 1063-28, 1063-34, and 1063-35 are weakly serpentinized harzburgites without visible veinlets or impregnation plagioclase grains; 1063-30 and I1063-32 are weakly serpentinized harzburgites with very thin rare amphibole–plagioclase veinlets; 1068-44 and 1068-45 are serpentinized lherzolites; 1068-24 is olivine–diopside poikilitic gabbro.

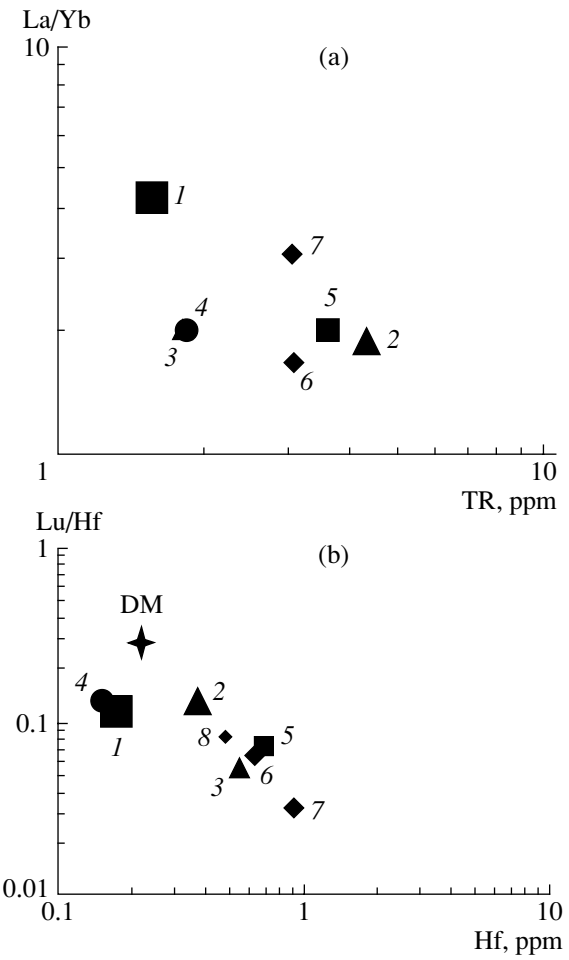

Fig. 9. Correlation between (a) the La/Yb ratio and the sum of REE and (b) Lu/Hf and Hf in harzburgites. DM is the depleted mantle. See Fig. 7 for symbol explanations.

analogous effect of the enrichment of the depleted harzburgites in incompatible trace elements and REE.

The petrography and composition of the ultramafics and plagiogranites led us to give preference to the explanation of their genesis that involves the effect of the interaction of the residue and the last melt portions that remained after the crystallization of the Fe–Ti gabbro. This explanation eliminates the need to invoke the action of melts coming from another deep-sitting ("plume") source, although such sources were proved to have existed beneath the Atlantic [22, 34, 37].

A closely similar effect of interaction between a residue and melt was documented for spinel lherzolite and harzburgite xenoliths in basalts, particularly if the ultramafics contained very thin veinlets consisting of plagioclase with minor amounts of amphibole, clinopyroxene, and, sometimes, biotite (see, for example, [34]). In these situations, the ultramafics are also enriched in LREE, and the rock–melt interaction is mineralogically pronounced only within the millimeter-thick contact zones of the veinlets. Such xenoliths of residual ultramafics are thought to have been torn by the melt from the walls of the magmatic chamber.

In the situation discussed in this publication, the newly formed generation of pyroxenes and Fe–Ti amphibole are also formed only along plagioclase veinlets, and all types of residual deformations in olivine and enstatite crystals intersected by veinlets were produced at subsolidus temperatures (including the superplastic flow that was responsible for the origin of linear zones of fine-grained olivine). This explanation can also account for the weak degree of serpentinization of the harzburgites, whose blocks could sometimes have been "shielded" by linear zones of stress relief (permeable zones). The zones along which melt percolation could later be inherited as pathways for the migration of aqueous fluids through the oceanic crust (as follows from the crystallization of talc and chlorite in veinlets) and, thus, hindered the development of reticulate serpentinization textures. We have, however, to admit that

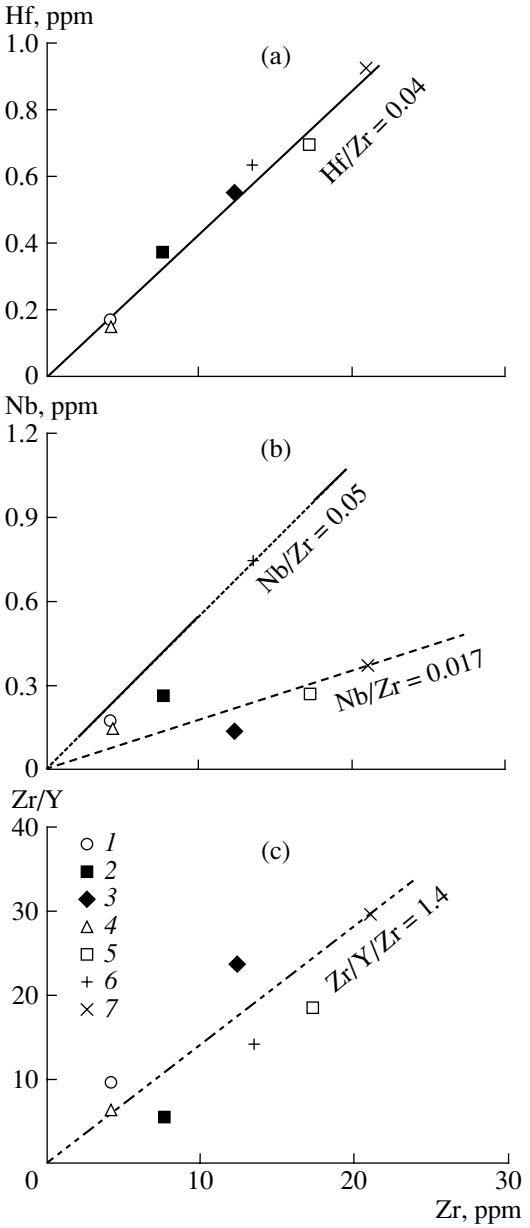

Fig. 10. Variations in the (a) Hf/Zr, (b) Nb/Zr, and (c) Zr/Y vs. Zr proportions in harzburgites. Numerals in the legend correspond to the sample numbers in Table 5: (*1*) I1063-28, (*2*) I1063-30, (*3*) I1063-32, (*4*) I1063-34, (*5*) I1063-35, (*6*) I1068-44, (*7*) I1068-45.

the fresh ultramafic rocks were brought to the seafloor quite recently and, thus, display practically no traces of submarine weathering.

The occurrence of serpentinized lherzolites and fresh harzburgites in the same vertical section of the modern oceanic crust calls for the specialized studying of the isotopic characteristics of these rocks, probably, including their radioisotopic dating. It seems to be reasonable to expect that this area of slow pulsating spreading can contain mantle residues of diverse ages.

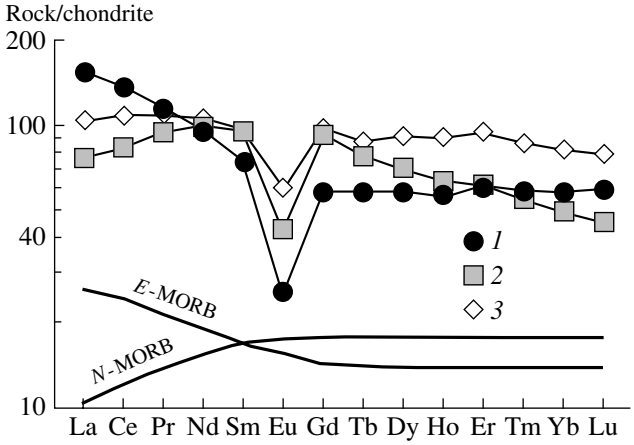

Fig. 11. Chondrite-normalized REE patterns of plagiogranites: (*1*) large vein of medium-grained plagiogranite in dolerite, sample I1060-57; (*2*) plagiogranite–granodiorite with resorbed gabbro relics, sample I1060-5; (*3*) thin veinlets of fine-grained plagiogranite in gabbro, sample I1063-18.

ACKNOWLEDGMENTS

The authors thank I.V. Chernyshev for help with chemical analyses and for the discussion of our results. A.Ya. Sharas'kin, L.V. Dmitriev, and S.A. Silant'ev are thanked for the constructive criticism of the manuscript and valuable comments. This study was financially supported by the Russian Foundation for Basic Research (project no. 02-05-64652) and the project "Oceanic Ore–Magmatic Systems: Parameters of Mineral-Forming Processes, Sources of Metals and Fluids, and Exploration Outlooks" within scope of Program "World Ocean: Seafloor Geology and Geodynamics, Marine Biology, and Ecology" of the Presidium of the Russian Academy of Sciences.

REFERENCES

1. A. A. Peive, G. N. Savel'eva, S. G. Skolotnev, and V. A. Simonov, "Tectonics and Origin of the Oceanic Crust in the Region of 'Dry' Spreading in the Central Atlantic (7°10–5° N)," Geotektonika, No. 2, 3–251 (2003) [Geotectonics **37**, 75–94 (2003)].
2. S. G. Skolotnev, N. S. Bortnikov, A. V. Peive, et al., "Geology of Ore-Hosting Rift Deeps near the Sierra Fracture Zone, Equatorial Atlantic," Dokl. Earth Sci. **391**, 679–684 (2003) [Dokl. Akad. Nauk **391**, 232–238 (2003)].
3. Yu. M. Pushcharovskii, N. S. Bortnikov, S. G. Skolotnev, et al., "Massive and Stringer-Disseminated Sulfide Mineralization in the Sierra Leone Fracture Zone of the Mid-Atlantic Ridge in Connection with Specific Features of Its Geological Structure," Dokl. Earth Sci. **384**, 357–361 (2002) [Dokl. Akad. Nauk **384**, 83–88 (2002)].
4. E. V. Sharkov, N. S. Bortnikov, O. A. Bogatikov, et al., "Mesozoic Zircon from Gabbronorites of the Axial Mid-Atlantic Ridge, 6° N, Markov Deep," Dokl. Earth Sci. **396**, 654–657 (2004) [Dokl. Akad. Nauk **396**, 675–677 (2004)].

5. L. V. Dmitriev, A. V. Ukhanov, and A. Ya. Sharas'kin, "Petrochemical Types of Mantle Peridotites," Geokhimiya, No. 8, 1160–1166 (1976).
6. M. Cannat and M. Seylier, "Transform Tectonic, Metamorphic Plagioclase and Amphibolization in Ultramafic Rocks of the Vema Transform Fault (Atlantic Ocean)," Earth Planet. Sci. Lett, **133**, 283–298 (1995).
7. Dick H.J. "Abyssal peridotites, very slow spreading ridges and ocean ridge magmatism." In: Saunders A.D. and Noris M.J., eds., Magmatism and ocean basins, Geol. Soc. of London, Spec. Publ., **42**, 71–105 (1989).
8. E. Bonatti and P. J. Michael, "Mantle Peridotites from Continental Rift to Ocean Basins to Subduction Zones," Earth Planet. Sci. Lett., **42**, 297–311 (1989).
9. M. Cannat, Y. Lagabrielle, H. Bougault, J. Case, et al., "Ultramafic and Gabbroic Exposures at the Mid-Atlantic Ridge: Geological Mapping in the 15°N Region," Tectonophysics **279**, 193–213 (1997).
10. A. A. Peive, K. O. Dobrolyubova, V. N. Efimov, et al., "Geological Features of the Sierra Leone Fracture Zone Region, Central Atlantic Ocean," Dokl. Earth Sci. **377**, 310–313 (2001) [Dokl. Akad. Nauk **377**, 803–806 (2001)].
11. P. Y. Michael, S. H. Langmure, H. J. Dick, et al., "Magmatic and Amagmatic Seafloor Generation at the Ultraslow-Spreading Gakkel Ridge Arctic Ocean," Nature **423**, 956–961 (2003).
12. Yu. M. Pushcharovskii, *Main Tectonic Features of the Southern Atlantic Ocean* (GEOS, Moscow, 2002) [in Russian].
13. G. B. Udintsev, N. A. Kurentsova, A. V. Kol'tsova, et al., "Topography and Structure of the Equatorial Segment of the Mid-Atlantic Ridge," Okeanologiya **36**, 897–909 (1996) [Oceanology **36**, 845–856 (1996)].
14. A. Peyve, E. Bonatti, D. Brunelli, et al., "New Data on Some Major MAR Structures: Initial Results of the R/V *Akademik Nikolaj Strakhov* Cruise 22," InterRidge News **9** (2), 28 (2000).
15. A. O. Mazarovich and S. Yu. Sokolov, "Hydrothermal Field in the Mid-Atlantic Ridge: Setting and Prospects for Further Discoveries," Russ. J. Earth Sci. **4**, 423–431 (2002).
16. A. O. Mazarovich, S. Yu. Sokolov, N. N. Turko, and K. O. Dobrolyubova, "Seafloor Topography and Structure of the Rift Zone of the Mid-Atlantic Ridge between 5° and 7°18' N," Russ. J. Earth Sci. **3** (5) (2001).
17. M. B. Baker and J. R. Beckett, "The Origin of Abyssal Peridotite: a Reinterpretation of Constraints Based on Primary Bulk Composition," Earth. Planet. Sci. Lett. **171**, 49–61 (1999).
18. Y. Niu, "Mantle Melting and Melt Extraction Processes beneath Ocean Ridges: Evidence from Abyssal Peridotites," J. Petrol. **385**, 326–329 (1997).
19. B. O. Mysen and A. L. Boettcher, "Melting of a Hydrous Mantle. II," J. Petrol. **16**, 520–548 (1975).
20. M. M. Hirshmann and E. M. Stolper, "A Possible Role for Garnet Pyroxenite in the Origin of the 'Garnet Signature' in MORB," Contrib. Mineral. Petrol. **124**, 85–208 (1996).
21. M. Godar, D. Josslin, and J.-L. Boudinier, "Relationships between Geochemistry and Structure Beneath a Paleo-Spreading Centre: A Study of the Mantle Section in the Oman Ophiolite," Earth Planet. Sci. Lett. **180**, 133–148 (2000).
22. S. A. Silantyev, "Variations in the Geochemical and Isotopic Characteristics of Residual Peridotites along the Mid-Atlantic Ridge as a Function of the Nature of the Mantle Magmatic Sources," Petrologiya **11**, 334–362 (2003) [Petrology **11**, 305–326 (2003)].
23. S. A. Silantyev, B. A. Bazylev, L. Dosso, et al., "Relation between Plume Magmatism and Mantle Metasomatism beneath the Mid-Atlantic Ridge: Petrological and Geochemical Evidence in Rocks of the Peridotite–Gabbro–Trondhjemite Association," Petrologiya **12**, 3–21 (2004) [Petrology **12**, 1–16 (2004)].
24. A. Prinzhofer and C. J. Allegre, "Residual Peridotites and the Mechanism of Partial Melting," Earth Planet. Sci. Lett. **74**, 251–265 (1985).
25. G. B. Piccardo, O. Muntener, A. Zanetti, et al., "The Lanzo South Peridotite: Melt/Peridotite Interaction in the Mantle Lithosphere of the Jurassic Ligurian Tethys," Ofioliti **29** (1), 37–62 (2004).
26. W. W. McDonough and F. A. Frey, "Rare Earth Elements in Upper Mantle Rocks," in *Geochemistry and Mineralogy of Rare Earth Elements*, Ed. by B. R. Lipin and G. A. McKay, Rev. Mineral. **21** (Mineral. Soc. Am., Washington DC, 1989), pp. 99–145.
27. S. S. Sun and W. R. McDonough, "Chemical and Isotopic Systematics of Oceanic Basalts: Implication for Mantle Composition and Processes," in *Magmatism in the Oceanic Basins*, Ed. by A. D. Saunders and M. J. Norry, (Geol. Soc., London, 1989), Vol. 42, pp. 313–345.
28. H.G. Wilshire, "Mantle Metasomatism: The REE Story," Geology **12**, 395–398 (1984).
29. D. L. Kohlstedt, C. Goetze, and W. B. Durham, "Experimental Deformation of Single Crystal Olivine with Application to Flow in the Mantle," in *Physics and Chemistry of Mineral and Rocks*, Ed. by R. G. J. Strens (Wileys, London, 1976), pp. 35–49.
30. A. Nicolas, J. L. Bouchez, F. Boudier, and J. C. Mercier, "Textures, Structures and Fabrics due to Solid State Flow in Some European Lherzolites," Tectonophysics **12**, 5–86 (1971).
31. A. Nicolas, *Structure of Ophiolites and Dynamics of Oceanic Lithosphere* (Kluwer, Dordrecht, 1989).
32. E. A. Denisova, "Ultramafic Mylonites of St. Paul Island, Equatorial Atlantic," Dokl. Akad. Nauk SSSR **319**, 1167–1172 (1991).
33. K. Ozawa and N. Shimizu, "Open-System Melting in the Upper Mantle: Constraints from the Hayachine–Miyamori Ophiolite, Northern Japan," J. Geophys. Res. **100** (B11), 315–322 (1995).
34. M. F. Roden and V. R. Murthy, "Mantle Metasomatism," Ann. Rev. Earth Planet. Sci. Lett. **13**, 269–296 (1985).
35. P. Tartarotti, S. Susini, P. Nimis, and L. Ottolini, "Melt Migration in the Upper Mantle along the Romanche Fracture Zone (Equatorial Atlantic)," Lithos, 125–149 (2002).
36. P. B. Keleman, H. J. B. Dick, and J. E. Quick, "Formation of Harzburgite by Pervasive Melt/Rock Reaction in the Upper Mantle," Nature **358**, 635–641 (1992).
37. L. V. Dmitriev, S. Yu. Sokolov, V. G. Melson, and T. O'Hearne, "Plume and Spreading Associations of Basalts in the Mid-Atlantic Ridge and Their Reflection in Petrological and Geophysical Characteristics," Ross. J. Earth Sci., **1**, 457–476 (1999).